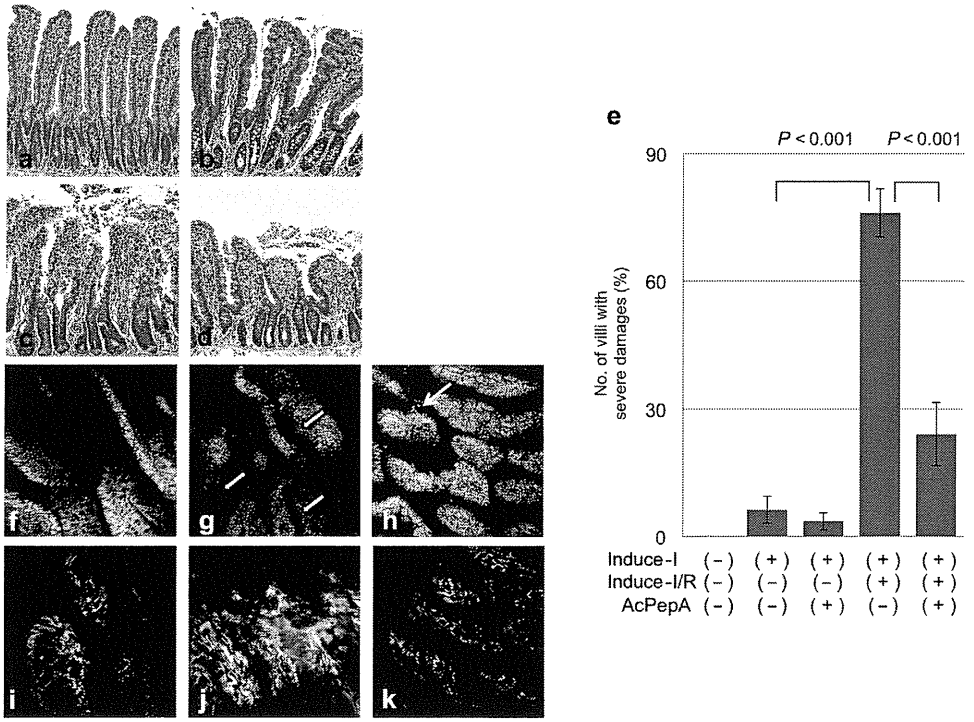

Fig. 1. Effect of AcPepA on the degree of small intestinal injury. Small intestinal injury (×600) was classified as (a) normal, (b) slight, (c) moderate and (d) severe. (e) The percentages of severely injured villi in the variously treated groups. *In vivo* histology images of the mucosal surface of distal rat ileum recorded under fluorescence confocal endomicroscopy (f, g, h) after i.v. administration of FITC-dextran and (i, j, k) topical administration of acridine orange. (f) Normal epithelium on the surface of the villi of the control group. (g) Longitudinal fissures on the surface of villi (white arrows) are apparent in the Induce-I/R group. (h) A few fissures on the surface of villi (thin white arrow) were observed in the Induce-I/R + AcPepA group. (i) Mucosal vasculature was normal in the control group. (j) Severe dye leakage from vessel lumina was observed 30 min after reperfusion in the Induce-I/R group. (k) Little dye leakage was observed in the Induce-I/R + AcPepA group.

Effects of AcPepA administration on proliferative changes in the epithelium with Induce-I/R

Because injuries to the small intestine change the resulted in a distributed balance between proliferation and apoptosis in the epithelium, the extent of proliferation of epithelial cells in the villi (except in strongly proliferative lesions) was examined to enable detection of small differences in the proliferation index (Fig. 2a). In normal villi, the PCNA index of the epithelium was 0.6–0.8% regardless of the treatment (Fig. 2b, c). In the injured villi, PCNA indices in the Induce-I group were similar to those observed in the Induce-I + AcPepA as well as in the Induce-I/R group (Fig. 2c). Administering AcPepA following Induce-I/R significantly increased the PCNA index compared with Induce-I/R without AcPepA administration (Fig. 2d, f). These results indicate that C5a inhibition by AcPepA alleviates I/R injury and increases cell proliferation in the epithelium.

Table 1. Degree of damage observed in intestinal villi

Intervention	No. of villi examined	No. of damaged villi (%)			
		Uninjured	Slightly	Moderately	Severely
Control	266	96	4	0	0
Induce-I	413	3	25	66	6
Induce-I + AcPep	436	2	47	47	4
Induce-I/R	289	0	2	22	76†
Induce-I/R + AcPep	417	0	14	62	24‡

†, $P < 0.001$ versus Induce-I/R
‡, $P < 0.001$ versus Induce-I

Induction of C5L2-positive PMNs in the villi

The localization of C5L2, a C5a receptor, was analyzed to identify cells in which C5a/C5L2 signaling is possibly transduced. Circulating inflammatory cells were often observed in dilated vessels located in the centers of villi, this phenomenon being associated with an inflammatory

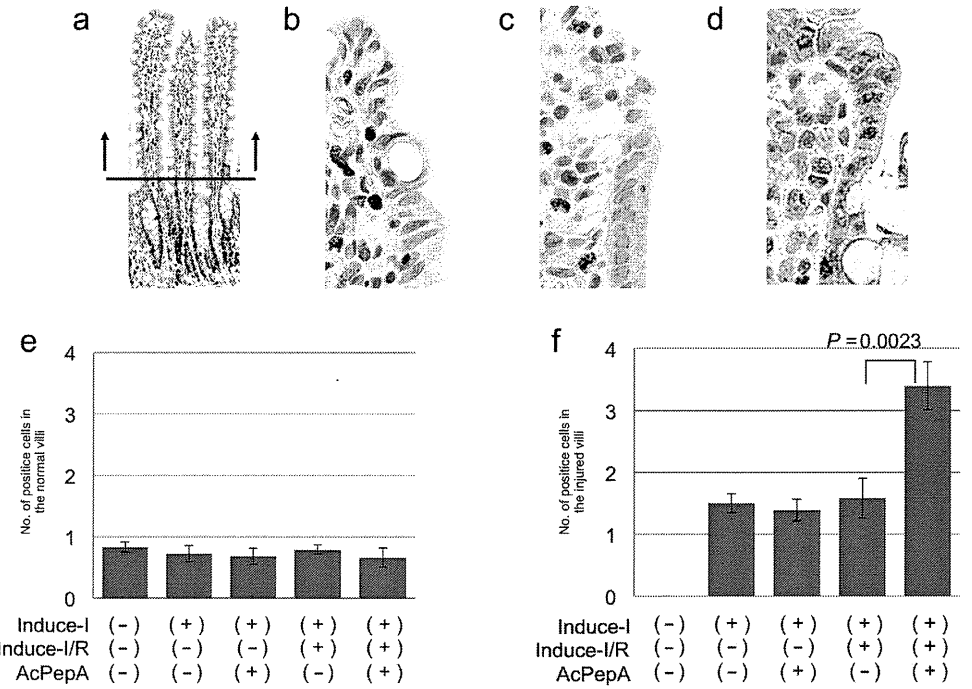

Fig. 2. Effect of AcPepA on proliferation of small intestinal epithelium. Recovery of the epithelium was evaluated by cell proliferation by counting PCNA-positive cells (PCNA index). (a) Positive epithelial cells were counted in the villi to avoid the strong proliferative region (below the horizontal bar in [a]) to facilitate detection of small differences in the cell proliferation index. Epithelial cells of injured small intestinal villi were visualized by PCNA staining of tissue from rats in the (b) Induce-I alone, (c) Induce-I/R and (d) Induce-I/R + AcPepA groups. (e) PCNA indices (number of positive cells in each villus) of the epithelium of normal and (f) injured villi are summarized.

response (square in Fig. 3a). C5L2-positive cells were observed among PMNs in the vessels (Fig. 3b). A few positive cells were observed outside the vessels such as in the erosion front of the injured villi (data not shown). $C5L2^{+}$PMNs were also observed in the dilated vessels of moderately or severely injured villi (Fig. 3c, d). The average number of $C5L2^{+}$PMNs was less than one in both the control and uninjured villi groups (Fig. 3E), the number of $C5L2^{+}$PMNs in the injured villi of the Induce-I/R group was significantly higher than in the Induce-I group. Additionally, $C5L2^{+}$PMNs were remarkably reduced by AcPepA administration in the Induce-I/R group (Fig. 3f). Because of our observation of a drastic increase in the number of C5L2-positive cells in vessels of the villi of the Induce-I/R group, C5a concentrations in the sera of the control, Induce-I/R and Induce-I/R + AcPepA groups were examined next (Fig. 3g). The serum concentration of C5a was 12 ng/mL in the control group, whereas in the Induce-I and Induce-I/R groups it was undetectable (Fig. 3g). An additional treatment with AcPepA restored the C5a concentration to >12 ng/mL, which is equivalent to that of the control group (Fig. 3g). These results suggest that C5a stimulates $C5L2^{+}$PMNs, causing a release of cytokines which exacerbate inflammation; thus, $C5L2^{+}$PMNs may contribute indirectly to I/R injury. Although Induce-I alone completely exhausted C5a in serum, Induce-I/R increased the C5a concentration up to 5 ng/mL, this possibly being attributable to further generation of C5a by reperfusion (R) following ischemia (I). The increased concentration of C5a (over 12 ng/mL) in rats treated with AcPepA following Induce-I/R may indicate protection of C5 by AcPepA from catabolism by an inhibitor of C5a, namely carboxypeptidase R (28, 29), which is also known as thrombin activatable fibrinolysis inhibitor.

Induction of CD68-positive macrophages in the villi

Next, evidence of macrophage induction in the control and injured villi was examined. In contrast with C5L2+PMNs, most CD68+MACs were observed in stromal lesions outside the vessels in slightly injured villi (arrowheads in Figure 4a). CD68+MACs were observed in the erosion fronts of the injured villi (arrowheads in Fig. 4b). Although many macrophages were observed with Induce-I/R (Fig. 4b), fewer were observed with Induce-I/R + AcPepA (Figure 4c). Regardless of the form of treatment, about one macrophage was observed

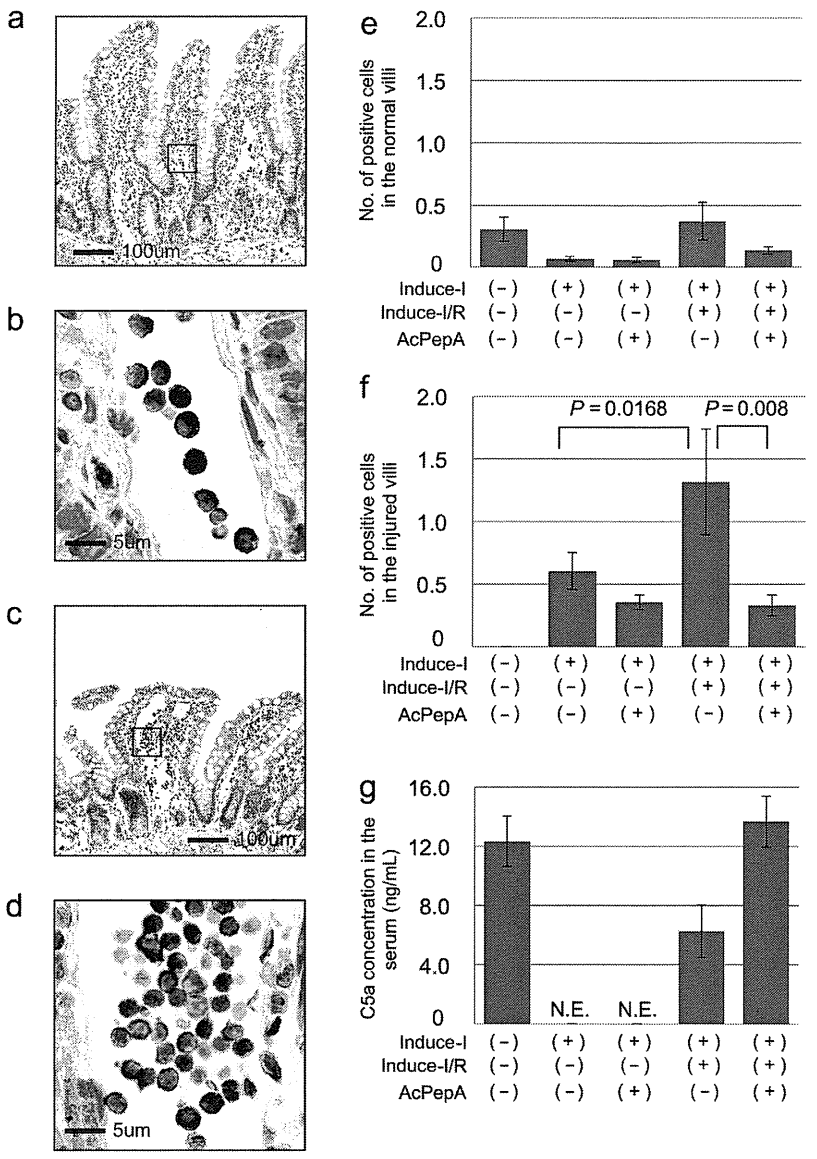

Fig. 3. Induction of C5L2-positive cells in villi. (a) Circulating inflammatory cells are often visible in dilated vessels located in the centers of the villi, this being associated with an inflammatory response (Square in 3a). (b) C5L2-positive cells among inflammatory cells in vessels. (c, d), C5L2-positive cells are also present in dilated vessels in severely injured villi. (e, f) The number of C5L2-positive cells in (e) normal and in (f) injured villi. (g) C5a serum concentrations were significantly lower in the Induce-I/R group than in the Induce-I/R + AcPepA group.

in each normal villus (Fig. 4d). In the injured villi, Induce-I/R significantly increased the number of macrophages, this effect being significantly suppressed by subsequent AcPepA administration (Fig. 4e). These results indicate that CD68+MACs are induced in the small intestine in association with I/R and play a direct role in I/R injury in a manner that is dependent on C5a activation.

Induction of CD204-positive macrophages in villi

CD204-positive macrophages are known to modulate inflammation by producing various cytokines; accordingly, their induction in villi was investigated. These cells were observed not only in stromal lesions outside vessels in slightly injured villi (arrowheads in Fig. 5a), but also infiltrating the erosion fronts of severely injured villi (Fig. 5b). Fewer CD204+MACs were observed in the Induce-I/R + AcPepA than in the Induce-I/R group (Fig. 5c), indicating that inhibition of C5a by AcPepA suppresses activation of macrophages. A mean of approximately one CD204+MAC was present in each control and uninjured villus (Fig. 5d). The average number of CD204+MACs was significantly larger in the uninjured villi of the Induce-I/R group than in those of the controls; additionally, AcPepA significantly decreased the number of CD204+MACs (Fig. 5d). In the injured villi, Induce-I/R induced significantly more numerous CD204+MACs than in the Induce-I alone

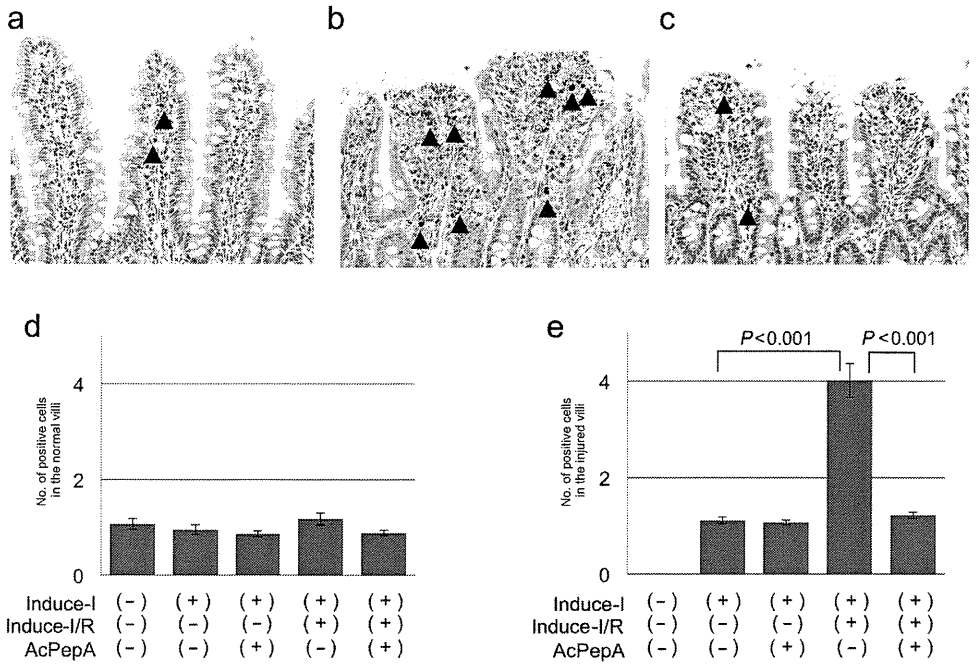

Fig. 4. Induction of macrophages in villi. (a) CD68-positive macrophages are present in the stromal region outside vessels in the villi (arrowheads). (b) CD68-positive macrophages are present in the erosion fronts of injured villi of rats in which I/R was induced (arrowheads). (c) Fewer macrophages are present in the Induce-I/R + AcPepA group. Numbers of the macrophages in (d) normal villi and (e) injured villi.

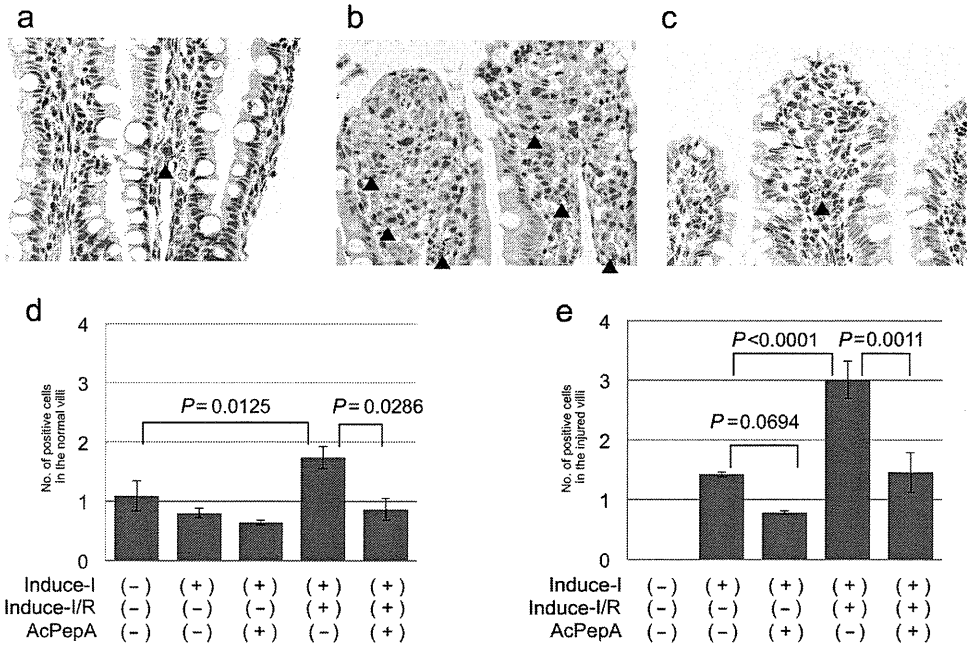

Fig. 5. Induction of CD204-positive macrophages in villi. (a) CD204-positive macrophages are present in the stromal region outside vessels in slightly injured villi (arrowheads). (b) CD204-positive macrophages are present in the erosion fronts of severely injured villi. (c) Fewer CD204-positive macrophages are present in the Induce-I/R + AcPepA group than in the Induce-I/R group. The number of CD204-positive macrophages in (d) normal and (e) injured villi.

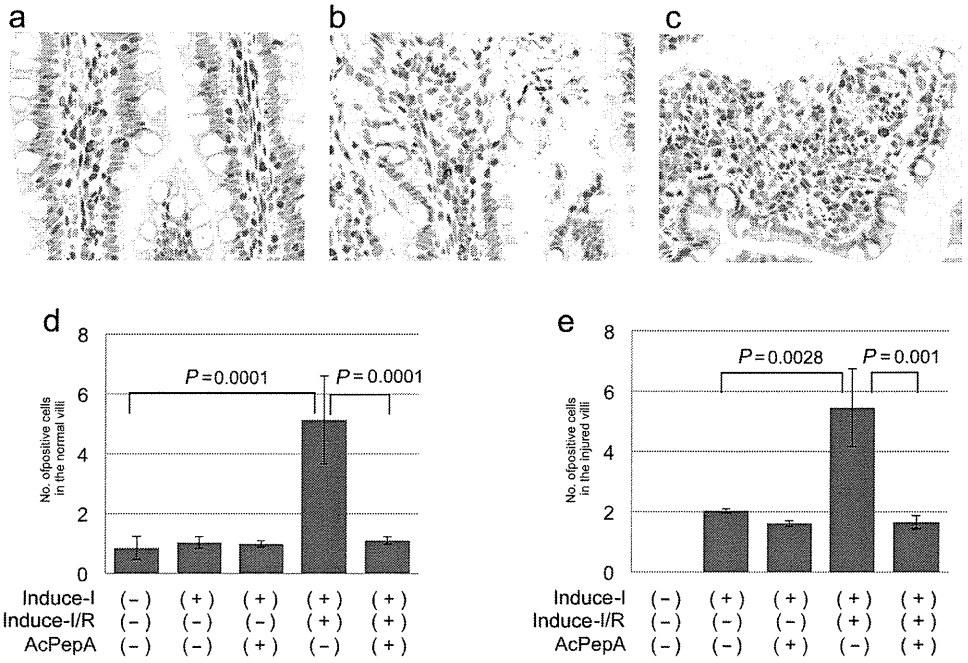

Fig. 6. Induction of HIF1-positive cells. (a, b) HIF1-α-positive cells are present in the stromal regions outside vessels in both (a) slightly injured and (b) moderately injured villi. (c) Many HIF1-α-positive cells are present in the erosion fronts of severely injured villi. (d, e) Changes in numbers of HIF1-α-positive cells in (d) normal and (e) injured villi.

group (Fig. 5e). There were significantly fewer positive cells in the AcPepA with Induce-I/R than in the Induce-I/R group alone; thus, again AcPepA with Induce-I tended to decrease their numbers (Fig. 5e). These results indicate that I/R induces significant CD204+MAC activation in injured villi and suggest that M2-type macrophages may contribute to I/R damage.

Induction of HIF-1α-positive cells

Hypoxia-induced factor 1-alpha is up-regulated in association with ischemic conditions. Therefore, whether HIF1-α-positive cells are involved in I/R-induced changes in the villi was investigated. HIF1-α-positive cells were detected by IHC both in stromal lesions outside vessels in slightly injured villi (Fig. 6a) and in moderately injured villi (Fig. 6b). Many HIF1-α-positive cells were observed in the erosion fronts of severely injured villi (Fig. 6c). The average number of HIF1-α-positive cells was similar to that of CD204+MACs in control, uninjured (Fig. 6d) and injured villi (Fig. 6e), suggesting that CD204+MACs produce HIF1-α.

DISCUSSION

Acute mesenteric ischemia is a serious multifactorial condition that develops from an occlusion of a main artery or vein. Interruption to the intestinal blood flow can lead to macro- and micro-circulatory failure of abrupt onset, frequently resulting in bowel necrosis (4). In this study, we designed an experimental setup for inducing severe injuries based on an AMI model that we had used previously (30–32). Similarly to in ileal specimens from AMI patients (33, 34), in our rat model we observed patchy evidence of damage to the villous mucosa, including detachment of cells, particularly in the villi's apical regions, giving rise to degraded mature epithelial cells in their lumens. We therefore evaluated the effects of I/R and the consequences of using a C5a antagonist to treat epithelial injury and examined regeneration using a clinically relevant experimental AMI protocol.

Acute mesenteric ischemia induces not only structural damage and circulatory deficiencies, but also leads to a great abundance of inflammatory mediators that can result in multi-organ failure (35). The complement system has been demonstrated to be a crucial mediator of I/R injury (36, 37). In the present study, we applied a newly synthesized C5a antagonist peptide, AcPepA (25, 27) and found that it significantly decreased the degree of I/R injury in our AMI model. Thus, we confirmed that C5a is involved in I/R injury in this model.

Because the C5a antagonist peptide AcPepA significantly decreased the degree of I/R damage in this study, we postulated that both structural damage to the villi and

repair of their intestinal epithelial cells would be induced by the inflammatory cytokines released from cells stimulated with C5a generated following complement activation. We therefore examined the cell proliferation activity of intestinal epithelial cells in normal and injured villi by counting the number of proliferating cells visualized by PCNA staining and found that AcPepA significantly increased proliferation of intestinal epithelial cells in injured villi. These results indicate that C5a restriction by AcPepA suppresses cytokine production by inflammatory cells, resulting in suppression of inflammation; any remaining C5a may have directly stimulated the growth of epithelial cells.

We have previously determined the localization of the C5a receptor C5L2 (38) to investigate how C5a/C5L2-mediated signaling modulates the inflammatory responses that lead to I/R injury (39, 40). It has been demonstrated *in vitro* that C5L2 is expressed in neutrophils, macrophages and fibroblasts (41). Additionally, C5a has been shown to exert a chemotactic effect on neutrophils (42), releasing superoxide anions from them. Thus, C5a is believed to be largely responsible for exacerbating PMN-mediated I/R tissue injuries. In the present study, C5a serum concentrations were decreased although C5L2+ PMNs were significantly more numerous in the Induce-I/R group, indicating that serum C5a is consumed because of greater binding to C5L2. It is also possible that the generated C5a is inactivated by carboxypeptidase R (28, 29), also known as thrombin activatable fibrinolysis inhibitor, which removes the carboxy-terminal arginine of C5a causing inactivation of the molecule, resulting in C5a-desArg. However, C5L2 + PMNs were observed mainly in vessels of the villi, a location somewhat distant from the site of epithelial injury. Thus, these results suggest that C5a/C5L signaling has an indirect influence on I/R damage. On the other hand, C5a has been shown to enhance release of pro-inflammatory cytokines from activated macrophages and monocytes (22, 43). Previous studies have suggested that alveolar macrophage activation is a key initiation signal for acute lung I/R injury (44, 45), whereas studies of complement inhibition in mice have suggested that intestinal I/R injury is unaffected by neutrophil depletion (36, 46). We found that CD68+MACs were significantly more numerous after I/R and decreased in number after subsequent AcPepA treatment. In addition, we mainly observed CD68+MACs near the site of injury. Taken together, even though there is some controversy about the direct contribution of neutrophils, C5a has an effect on PMNs and the subsequent activation of macrophages plays an important role in small intestinal I/R injury.

Several studies have demonstrated that M2 type macrophages produce cytokines such as TNF-α, IL-6 and IL-12 in response to inflammatory stimuli (47–49); M2 macrophages are considered to be important effectors of fatal cellular mechanisms during cancer-related inflammation. CD204, a class A scavenger receptor, is a multifunctional molecule that is expressed in M2 macrophages. We postulated that CD204+MACs, which produce HIF1-α, are involved in I/R injury. In the present study, I/R treatment significantly increased the number of CD204+MACs in both injured and normal villi. Again, this increase was suppressed by AcPepA treatment, which suggests that CD204+MACs are indeed activated in response to I/R.

Hypoxia-induced factor 1-alpha is a heterodimeric transcription factor composed of a constitutively expressed alpha-subunit (50) and is important for promoting a variety of cellular responses to hypoxia (51). Induce-I/R would be expected to activate HIF1-α; however, its role in I/R injury is controversial. The protective role of HIF1-α in I/R injury has been demonstrated in proximal tubule cells in the kidney (52--54) as well as in astrocytes (55); additionally, HIF1- α expression is known to be essential for the development of I/R injury in the gut, especially with prolonged ischemia (56, 57). In the present study, I/R significantly increased the number of HIF1-α-positive cells in both injured and uninjured villi. Induction of CD204+MACs correlated closely with the number of HIF1-α-positive cells and both types of cells were suppressed by AcPepA treatment. These results suggest that, on activation with treatment I/R, C5a directly or indirectly induces activation of CD204+MACs in the intestinal villi; these cells then secrete HIF1-α.

The mechanisms for I/R injury involve cellular/molecular processes that begin with hypoxia and hypoxia-induced C5a formation; concerted communication between C5a, MACs and PMNs is necessary for the mediation of I/R damage in the villi. We propose that activated leukocytes flowing into the villus microcirculation spread signals further towards resident macrophages in the lamina propria and that this leads to stimulation of macrophage-derived HIF-1α production at the injury site. According to the outlined scenario, the greatest structural destruction would be expected to occur when C5a, activated PMNs and MACs are all present in the reperfused villi. Furthermore, this cellular casting might also explain the patchy pattern of mucosal damage; the damage is less severe if one or more of the players is not present or inactive.

Several studies have used blocking antibodies or inhibitors to target C5 or C5a. In I/R models of rat intestine, both C5 and C5a blockade result in protection

from I/R injury (16, 58, 59). In myocardial infarcts in rats, antibodies to C5 significantly inhibit necrosis, cell apoptosis and neutrophil infiltration (60). In pigs, use of antibodies directed against C5a results in reduced myocardial injury and reduced coronary endothelial dysfunction after I/R (61, 62). AcPepA, which we generated as an inhibitory C5a peptide, is effective in reducing the incidence of lethal shock in rats (25) and mice (27), as well as sepsis induced by lethal doses of bacterial LPS in cynomolgus monkeys (26). In the present study, we demonstrated that AcPepA suppressed I/R tissue injury in our AMI rat model. Combined together, targeting C5/C5a may represent the best strategy for inhibiting complement-mediated I/R-induced tissue injury and may therefore prove useful for therapeutic interventions in clinical settings. These experimental studies should lead to clinical trials in patients with AMI, lethal shock and sepsis.

In summary, we examined the mechanisms of C5a-induced I/R injury using our clinically relevant rat AMI model. The proposed mechanism includes the effect of C5a on PMNs and the subsequent induction of CD204+MACs, which secrete HIF1-α, in the intestinal villi. Overall, targeting of C5/C5a is a potential strategy for inhibiting PMNs and reducing macrophage- mediated I/R injury and may therefore be a good option for future therapeutic interventions.

ACKNOWLEDGEMENTS

The authors are grateful to Nikolett Beretka, Csilla Mester, Anita Németh, Károly Tóth and Kálmán Vas for their skillful assistance. The study was supported by Hungarian Science Research Fund (OTKA) grants K104656 and Social Renewal Operational Programme (TÁMOP)-4.2.2/A-11/1/KONV-2012-0035 and a grant in aid for JST Research Grant A-STEP (AS2316910G) and Scientific Support Programs for Cancer Research Grant-in-Aid for Scientific Research on Innovative Areas Ministry of Education, Culture, Sports, Science and Technology in Japan.

DISCLOSURE

The authors have no conflict of interest to declare.

REFERENCES

1. Wilson C., Gupta R., Gilmour, D.G., Imrie, C.W. (1987) Acute superior mesenteric ischaemia. *Br J Surg* **74**: 279–81.
2. Oldenburg W.A., Lau L.L., Rodenberg T.J., Edmonds H.J., Burger, C.D. (2004) Acute mesenteric ischemia: A clinical review. *Arch Intern Med* **164**: 1054–62.
3. Benjamin E., Oropello, J.M., Iberti, T.J. (1993) Acute mesenteric ischemia: pathophysiology, diagnosis, and treatment. *Dis Mon* **39**: 131–210.
4. Berland T., Oldenburg W.A. (2008) Acute mesenteric ischemia. *Curr Treat Options Gastroenterol* **11**: 3–10.
5. Rijke R.P., Van Der Meer-Fieggen W., Galjaard H. (1974) Effect of villus length on cell proliferation and migration in small intestinal epithelium. *Cell Tissue Kinet* **7**: 577–86.
6. Yasue N., Guth P.H. (1988) Role of exogenous acid and retransfusion in hemorrhagic shock-induced gastric lesions in the rat. *Gastroenterology* **94**: 1135–43.
7. Noda T., Iwakiri R., Fujimoto K., Matsuo S., Aw, T.Y. (1998) Programmed cell death induced by ischemia-reperfusion in rat intestinal mucosa. *Am J Physiol* **274**: G270–6.
8. Ikeda H., Suzuki Y., Suzuki M., Koike M., Tamura J., Tong J., Nomura M., Itoh G. (1998) Apoptosis is a major mode of cell death caused by ischaemia and ischaemia/reperfusion injury to the rat intestinal epithelium. *Gut* **42**: 530–7.
9. Carter M.B., Wilson M.A., Wead W.B., Garrison R.N. (1996) Platelet-activating factor mediates pulmonary macromolecular leak following intestinal ischemia-reperfusion. *J Surg Res* **60**: 403–8.
10. Yao Y.M., Sheng Z.Y., Yu Y., Tian H.M., Wang Y.P., Lu L.R., Xu S.H. (1995) The potential etiologic role of tumor necrosis factor in mediating multiple organ dysfunction in rats following intestinal ischemia-reperfusion injury. *Resuscitation* **29**: 157–68.
11. Tamion F., Richard V., Lyoumi S., Daveau M., Bonmarchand G., Leroy J., Thuillez C., Lebreton J.P. (1997) Gut ischemia and mesenteric synthesis of inflammatory cytokines after hemorrhagic or endotoxic shock. *Am J Physiol* **273**: G314–21.
12. Parks D.A., Bulkley G.B., Granger D.N., Hamilton S.R., McCord J.M. (1982) Ischemic injury in the cat small intestine: Role of superoxide radicals. *Gastroenterology* **82**: 9–15.
13. Riedemann N.C., Ward P.A. (2003) Complement in ischemia reperfusion injury. *Am J Pathol* **162**: 363–7.
14. Heller T., Hennecke M., Baumann U., Gessner J.E., Zu Vilsendorf A.M., Baensch M., Boulay F., Kola A., Klos A., Bautsch W., Kohl J. (1999) Selection of a C5a receptor antagonist from phage libraries attenuating the inflammatory response in immune complex disease and ischemia/reperfusion injury. *J Immunol* **163**: 985–94.
15. Kimura T., Andoh A., Fujiyama Y., Saotome T., Bamba T. (1998) A blockade of complement activation prevents rapid intestinal ischaemia-reperfusion injury by modulating mucosal mast cell degranulation in rats. *Clin Exp Immunol* **111**: 484–90.
16. Wada K., Montalto M.C., Stahl G.L. (2001) Inhibition of complement C5 reduces local and remote organ injury after intestinal ischemia/reperfusion in the rat. *Gastroenterology* **120**: 126–33.
17. Van Beek J., Bernaudin M., Petit E., Gasque P., Nouvelot, A., Mackenzie E.T., Fontaine M. (2000) Expression of receptors for complement anaphylatoxins C3a and C5a following permanent focal cerebral ischemia in the mouse. *Exp Neurol* **161**: 373–82.
18. Bremer C., Bradford B.U., Hunt K.J., Knecht K.T., Connor H.D., Mason R.P., Thurman R.G. (1994) Role of Kupffer cells in the pathogenesis of hepatic reperfusion injury. *Am J Physiol* **267**: G630–6.
19. Henrion J. (2000) Ischemia/reperfusion injury of the liver: pathophysiologic hypotheses and potential relevance to human hypoxic hepatitis. *Acta Gastroenterol Belg* **63**: 336–47.
20. Wanner G.A., Ertel W., Muller P., Hofer Y., Leiderer R., Menger M.D., Messmer K. (1996) Liver ischemia and

reperfusion induces a systemic inflammatory response through Kupffer cell activation. *Shock* **5**: 34–40.
21. Cavaillon J.M., Fitting C., Haeffner-Cavaillon N. (1990) Recombinant C5a enhances interleukin 1 and tumor necrosis factor release by lipopolysaccharide-stimulated monocytes and macrophages. *Eur J Immunol* **20**: 253–7.
22. Haynes D.R., Harkin D.G., Bignold L.P., Hutchens M.J., Taylor S.M., Fairlie D.P. (2000) Inhibition of C5a-induced neutrophil chemotaxis and macrophage cytokine production *in vitro* by a new C5a receptor antagonist. *Biochem Pharmacol* **60**: 729–33.
23. Tyagi S., Klickstein L.B., Nicholson-Weller A. (2000) C5a-stimulated human neutrophils use a subset of beta2 integrins to support the adhesion-dependent phase of superoxide production. *J Leukoc Biol* **68**: 679–86.
24. Okada N., Imai M., Okada A., Ono F., Okada H. (2011) HMGB1 release by C5a anaphylatoxin is an effective target for sepsis treatment. *natureprecedings* hdl:10101/npre.2011.5727.1.
25. Fujita E., Farkas I., Campbell W., Baranyi L., Okada H., Okada N. (2004) Inactivation of C5a anaphylatoxin by a peptide that is complementary to a region of C5a. *J Immunol* **172**: 6382–7.
26. Okada H., Imai M., Ono F., Okada A., Tada T., Mizue Y., Terao K., Okada N. (2011) Novel complementary peptides to target molecules. *Anticancer Res* **31**: 2511–6.
27. Okada N., Asai, S., Hotta A., Miura N., Ohno N., Farkas I., Hau, L., Okada H. (2007) Increased inhibitory capacity of an anti-C5a complementary peptide following acetylation of N-terminal alanine. *Microbiol Immunol* **51**: 439–43.
28. Campbell W., Okada H. (1989) An arginine specific carboxypeptidase generated in blood during coagulation or inflammation which is unrelated to carboxypeptidase N or its subunits. *Biochem Biophys Res Commun* **162**: 933–9.
29. Campbell W.D., Lazoura E., Okada N., Okada H. (2002) Inactivation of C3a and C5a octapeptides by carboxypeptidase R and carboxypeptidase *N*. *Microbiol Immunol* **46**: 131–4.
30. Szabo A., Vollmar B., Boros M., Menger, M.D. (2008) *In vivo* fluorescence microscopic imaging for dynamic quantitative assessment of intestinal mucosa permeability in mice. *J Surg Res* **145**: 179–85.
31. Boros M., Ghyczy M., Erces D., Varga, G., Tokes T., Kupai, K., Torday C., Kaszaki J. (2012) The anti-inflammatory effects of methane. *Crit Care Med* **40**: 1269–78.
32. Adamicza A., Kaszaki J., Boros M., Hantos Z. (2012) Pulmonary mechanical responses to intestinal ischaemia-reperfusion and endotoxin preconditioning. *Acta Physiol Hung* **99**: 289–301.
33. Chiu C.J., Mcardle A.H., Brown R., Scott H.J., Gurd F.N. (1970) Intestinal mucosal lesion in low-flow states. I. A morphological, hemodynamic, and metabolic reappraisal. *Arch Surg* **101**: 478–83.
34. Thuijls G., Van Wijck K., Grootjans J., Derikx J.P., Van Bijnen A.A., Heineman E., Dejong C.H., Buurman W.A., Poeze M. (2011) Early diagnosis of intestinal ischemia using urinary and plasma fatty acid binding proteins. *Ann Surg* **253**: 303–8.
35. Roumen R.M., Redl H., Schlag G., Zilow G., Sandtner W., Koller W., Hendriks T., Goris R.J. (1995) Inflammatory mediators in relation to the development of multiple organ failure in patients after severe blunt trauma. *Crit Care Med* **23**: 474–80.
36. Austen W.G., Jr., Kyriakides C., Favuzza J., Wang Y., Kobzik L., Moore F.D., Jr., Hechtman H.B. (1999) Intestinal ischemia-reperfusion injury is mediated by the membrane attack complex. *Surgery* **126**: 343–8.
37. De Vries B., Kohl J., Leclercq W.K., Wolfs T.G., Van Bijnen A.A., Heeringa P., Buurman W.A. (2003) Complement factor C5a mediates renal ischemia-reperfusion injury independent from neutrophils. *J Immunol* **170**: 3883–9.
38. Bamberg C.E., Mackay C.R., Lee H., Zahra D., Jackson J., Lim Y.S., Whitfeld P.L., Craig S., Corsini E., Lu B., Gerard C., Gerard N.P. (2010) The C5a receptor (C5aR) C5L2 is a modulator of C5aR-mediated signal transduction. *J Biol Chem* **285**: 7633–44.
39. Hawlisch H., Belkaid Y., Baelder R., Hildeman D., Gerard C., Kohl J. (2005) C5a negatively regulates toll-like receptor 4-induced immune responses. *Immunity* **22**: 415–26.
40. Hopken U.E., Lu B., Gerard N.P., Gerard C. (1996) The C5a chemoattractant receptor mediates mucosal defence to infection. *Nature* **383**: 86–9.
41. Chen N.J., Mirtsos C., Suh D., Lu Y.C., Lin W.J., Mckerlie C., Lee T., Baribault H., Tian H., Yeh W.C. (2007) C5L2 is critical for the biological activities of the anaphylatoxins C5a and C3a. *Nature* **446**: 203–7.
42. Shin H.S., Snyderman R., Friedman E., Mellors A., Mayer M.M. (1968) Chemotactic and anaphylatoxic fragment cleaved from the fifth component of guinea pig complement. *Science* **162**: 361–3.
43. Okusawa S., Yancey K.B., Van Der Meer J.W., Endres S., Lonnemann G., Hefter K., Frank M.M., Burke J.F., Dinarello C.A., Gelfand J.A. (1988) C5a stimulates secretion of tumor necrosis factor from human mononuclear cells *in vitro*. Comparison with secretion of interleukin 1 beta and interleukin 1 alpha. *J Exp Med* **168**: 443–8.
44. Amaral F.A., Fagundes C.T., Guabiraba R., Vieira A.T., Souza A.L., Russo R.C., Soares M.P., Teixeira M.M., Souza D.G. (2007) The role of macrophage migration inhibitory factor in the cascade of events leading to reperfusion-induced inflammatory injury and lethality. *Am J Pathol* **171**: 1887–93.
45. Zhao M., Fernandez L.G., Doctor A., Sharma A.K., Zarbock A., Tribble C.G., Kron I.L., Laubach V.E. (2006) Alveolar macrophage activation is a key initiation signal for acute lung ischemia-reperfusion injury. *Am J Physiol Lung Cell Mol Physiol* **291**: L1018–26.
46. Rehrig S., Fleming S.D., Anderson J., Guthridge J.M., Rakstang J., Mcqueen C.E., Holers V.M., Tsokos G.C., Shea-Donohue T. (2001) Complement inhibitor, complement receptor 1-related gene/protein y-Ig attenuates intestinal damage after the onset of mesenteric ischemia/reperfusion injury in mice. *J Immunol* **167**: 5921–7.
47. Haworth R., Platt N., Keshav S., Hughes D., Darley E., Suzuki H., Kurihara Y., Kodama T., Gordon S. (1997) The macrophage scavenger receptor type A is expressed by activated macrophages and protects the host against lethal endotoxic shock. *J Exp Med* **186**: 1431–9.
48. Beamer C.A., Holian A. (2005) Scavenger receptor class A type I/II (CD204) null mice fail to develop fibrosis following silica exposure. *Am J Physiol Lung Cell Mol Physiol* **289**: L186–95.
49. Coller S.P., Paulnock D.M. (2001) Signaling pathways initiated in macrophages after engagement of type A scavenger receptors. *J Leukoc Biol* **70**: 142–8.
50. Semenza G.L. (2001) HIF-1 and mechanisms of hypoxia sensing. *Curr Opin Cell Biol* **13**: 167–71.
51. Weidemann A., Johnson R.S. (2008) Biology of HIF-1alpha. *Cell Death Differ* **15**: 621–7.
52. Bernhardt W.M., Campean V., Kany S., Jurgensen J.S., Weidemann A., Warnecke C., Arend M., Klaus S., Gunzler V., Amann K., Willam C., Wiesener M.S., Eckardt K.U. (2006) Preconditional activation of hypoxia-inducible factors

ameliorates ischemic acute renal failure. *J Am Soc Nephrol* **17**: 1970–8.
53. Hill P., Shukla D., Tran M.G., Aragones J., Cook H.T., Carmeliet P., Maxwell P.H. (2008) Inhibition of hypoxia inducible factor hydroxylases protects against renal ischemia-reperfusion injury. *J Am Soc Nephrol* **19**: 39–46.
54. Manotham K., Tanaka T., Ohse T., Kojima I., Miyata T., Inagi R., Tanaka H., Sassa R., Fujita T., Nangaku M. (2005) A biologic role of HIF-1 in the renal medulla. *Kidney Int* **67**: 1428–39.
55. Du F., Zhu L., Qian Z.M., Wu X.M., Yung W.H., Ke Y. (2010) Hyperthermic preconditioning protects astrocytes from ischemia/reperfusion injury by up-regulation of HIF-1 alpha expression and binding activity. *Biochim Biophys Acta* **1802**: 1048–53.
56. Sutton T.A., Wilkinson J., Mang H.E., Knipe N.L., Plotkin Z., Hosein M., Zak K., Wittenborn J., Dagher P.C. (2008) p53 regulates renal expression of HIF-1{alpha} and pVHL under physiological conditions and after ischemia-reperfusion injury. *Am J Physiol Renal Physiol* **295**: F1666–77.
57. Feinman R., Deitch E.A., Watkins A.C., Abungu B., Colorado I., Kannan K.B., Sheth S.U., Caputo F.J., Lu Q., Ramanathan M., Attan S., Badami C.D., Doucet D., Barlos D., Bosch-Marce M., Semenza G.L., Xu D.Z. (2010) HIF-1 mediates pathogenic inflammatory responses to intestinal ischemia-reperfusion injury. *Am J Physiol Gastrointest Liver Physiol* **299**: G833–43.
58. Arumugam T.V., Shiels I.A., Woodruff T.M., Reid R.C., Fairlie D.P., Taylor S.M. (2002) Protective effect of a new C5a receptor antagonist against ischemia-reperfusion injury in the rat small intestine. *J Surg Res* **103**: 260–7.
59. Hill J., Lindsay T.F., Ortiz F., Yeh C.G., Hechtman H.B., Moore F.D., Jr. (1992) Soluble complement receptor type 1 ameliorates the local and remote organ injury after intestinal ischemia-reperfusion in the rat. *J Immunol* **149**: 1723–8.
60. Vakeva A.P., Agah A., Rollins S.A., Matis L.A., Li L., Stahl G.L. (1998) Myocardial infarction and apoptosis after myocardial ischemia and reperfusion: Role of the terminal complement components and inhibition by anti-C5 therapy. *Circulation* **97**: 2259–67.
61. Tofukuji M., Stahl G.L., Agah A., Metais C., Simons M., Sellke F.W. (1998) Anti-C5a monoclonal antibody reduces cardiopulmonary bypass and cardioplegia-induced coronary endothelial dysfunction. *J Thorac Cardiovasc Surg* **116**: 1060–8.
62. Amsterdam E.A., Stahl G.L., Pan H.L., Rendig S.V., Fletcher M.P., Longhurst J.C. (1995) Limitation of reperfusion injury by a monoclonal antibody to C5a during myocardial infarction in pigs. *Am J Physiol* **268**: H448–57.

In vivo ^{18}F-fluorodeoxyglucose-positron emission tomography/computed tomography imaging of pancreatic tumors in a transgenic rat model carrying the human *KRAS*^{G12V} oncogene

KOJI SHIBATA[1,2], KATSUMI FUKAMACHI[1], ATSUSHI TSUJI[3], TSUNEO SAGA[3], MITSURU FUTAKUCHI[1], MASATO NAGINO[2], HIROYUKI TSUDA[4] and MASUMI SUZUI[1]

[1]Department of Molecular Toxicology, Nagoya City University Graduate School of Medical Sciences and Medical School, Nagoya, Aichi 467-8601; [2]Division of Surgical Oncology, Department of Surgery, Nagoya University Graduate School of Medicine, Nagoya, Aichi 466-8550; [3]Diagnostic Imaging Program, Molecular Imaging Center, National Institute of Radiological Sciences, Chiba, Chiba 263-8555; [4]Laboratory of Nanotoxicology Project, Nagoya University, Nagoya, Aichi 467-8603, Japan

Received March 25, 2014; Accepted December 19, 2014

DOI: 10.3892/ol.2015.3053

Abstract. A novel *KRAS*-mediated transgenic rat model has previously been demonstrated, in which animals develop multiple pancreatic ductal adenocarcinoma (PDAC) that is histologically similar to human PDAC within two weeks. Positron emission tomography (PET)/computed tomography (CT) is commonly used for the diagnosis and staging of PDAC in humans, and can be adopted for optimal use in animal experiments. The aim of the present study was to evaluate the carcinogenic process in a rat pancreatic carcinoma model using small-animal multimodality imaging systems. The utility of fluorodeoxyglucose (FDG)-PET/CT in detecting the location and size of PDAC during tumor development in the present transgenic rat model was assessed. A small animal multimodality PET/CT system and contrast-enhanced CT (CECT) system were used for the imaging analysis of *KRAS*^{G12V} male transgenic rats (n=6), which developed pancreatic tumors following the administration of an injection of Cre recombinase (Cre)-carrying adenovirus. Laparotomies performed at six weeks post-treatment revealed that all three (100%) Cre-expressing rats developed pancreatic tumors that were <2 mm in diameter, none of which were detected by ^{18}F-FDG PET/CT or CECT. At eight weeks post-treatment, the pancreatic tumors were heterogeneously visualized by ^{18}F-FDG-PET/CT and CECT in two of the three rats. Furthermore, the autopsies confirmed that all three rats had developed pancreatic tumors. These novel findings provide evidence that the FDG-PET/CT imaging system is a valuable tool for the evaluation of the carcinogenic process, and one which may aid in treatment and preventive methods for pancreatic tumors in mammalian models. A limitation associated with the early detection of PDACs warrants further investigation.

Correspondence to: Dr Masumi Suzui, Department of Molecular Toxicology, Nagoya City University Graduate School of Medical Sciences and Medical School, 1 Kawasumi, Mizuho-cho, Mizuho-ku, Nagoya, Aichi 467-8601, Japan
E-mail: suzui@med.nagoya-cu.ac.jp

Key words: carcinogenesis, positron emission tomography/computed tomography, ^{18}F-fluorodeoxyglucose, laparotomy, pancreatic tumor, rat model

Introduction

With >250,000 annual mortalities, pancreatic carcinoma is one of the most lethal malignancies, ranking 12th worldwide (1). Mortality resulting from this disease is high even in developed countries, including Japan, the United Kingdom, France and the United States (2,3). Overall, >75% of pancreatic carcinoma cases are histologically characterized as pancreatic ductal adenocarcinoma (PDAC) (4,5). The majority of cases of PDAC are incurable due to the necessity of extensive resection, which is often not feasible, and due to the fact that the disease is rarely identified at an early stage. Furthermore, the majority of patients with advanced PDAC either do not respond, or respond transiently to chemotherapeutic drugs and radiation (6). Typically, the majority of patients with PDAC succumb to the disease within one year of diagnosis, and the overall five-year survival rate is <5% (7). Even in patients with resectable carcinoma, the long-term outcome remains unsatisfactory due to the incidence of early recurrence following surgical resection.

In order to gain an improved understanding of this lethal malignant carcinoma, studies that use animal PDAC models with pancreatic neoplasms that resemble human PDAC are usually desirable. By focusing on human pancreatic adenocarcinomas that express a high frequency of *KRAS* mutation, a transgenic rat model carrying the human *HRAS*^{G12V} or *KRAS*^{G12V} oncogene was established (8,9). The activation of the target transgene is attained by the injection of a Cre recombinase (Cre)-carrying adenovirus into the pancreatic ducts of the animal via the

common bile duct (8,9). In this model, the transgenic rats usually develop pre-neoplastic and neoplastic pancreatic lesions within two weeks of the viral inoculation (10). These lesions in the transgenic rats exhibit morphological similarities to those observed in human pancreatic lesions, including PDAC (11) and intraepithelial neoplasias (PanINs) (9).

Due to the position of the tumors within the abdominal cavity, laparotomy is the only technique that is able to determine the existence and size of pancreatic tumors within the transgenic rats following virus inoculation, as the tumors cannot be visually assessed from surface scans of the affected rats. A previous study determined that in order to serologically detect early-stage PDAC in the rat models, serum N-ERC levels and the levels of several serum miRNAs, which are expressed differentially in PDAC transgenic rats and control rats, could be used (8,12). However, even in the case of elevated levels of high serum biomarkers, the exact location and size of pancreatic tumors is difficult to detect unless exploratory surgery is performed within the abdominal cavity.

^{18}F-fluorodeoxyglucose-positron emission tomography ([^{18}F-FDG-PET) is commonly used during the diagnosis of pancreatic tumors (13,14). Due to a high sensitivity and penetration depth, PET is considered to be more accurate for the detection and identification of metastases in humans and animal models than other imaging systems (15,16).

The objective of the present study was to evaluate the carcinogenic process in a mammalian model using imaging modalities, such as PET/computed tomography (CT), which are applicable for the study of human PDAC.

Materials and methods

Animals. In total, six male *KRAS*^{G12V} oncogene transgenic rats were used in the present study. Routine genotyping was performed as previously described (8). The rats were kept in plastic cages in an air-conditioned room at 24±2˚C and 60±5% humidity with a 12-h light/12-hour dark cycle. A basal diet (Oriental Yeast Co., Ltd., Tokyo, Japan) and tap water were available *ad libitum* throughout the experiment. All experiments were approved by the Animal Care and Use Committee of Nagoya City University Graduate School of Medical Sciences and the National Institute of Radiological Sciences (Tokyo, Japan).

Procedure of adenovirus inoculation. The preparation and inoculation of the adenoviruses was performed as previously described (9). In brief, a Cre-recombinase expressing adenovirus was amplified in HEK293 cells and then purified using the Vivapure AdenoPACK (Vivascience, Hannover, Germany) (17). The titer of the adenovirus was then determined using an Adeno-X rapid titer kit (Clontech, Mountain View, CA, USA). The virus was prepared to a concentration of 4.0×10^9 plaque-forming units/ml. The virus (300-400 μl) was injected using a small syringe into the pancreatic duct of the rats as previously described (9).

[^{18}F-FDG-PET and CT procedures, and image analysis. The time course of the experimental protocol is shown in Fig. 1. For the present study, 10-week-old male *KRAS*^{G12V} transgenic rats were used. The rats were divided into two groups, with three rats per group. The rats in groups 1 and 2 were administered with the Cre-expressing adenovirus vector or an empty vector (negative control), respectively. A small-animal multimodality PET system (Inveon; Siemens Healthcare Inc., Malvern, PA, USA) was used for PET data acquisition. Following an overnight fast, each rat (body weight, 403-583 g) was injected with 15 MBq (14.6±1.6 MBq) ^{18}F-FDG (Nihon Medi-Physics Co., Ltd., Tokyo, Japan) via the tail vein, whilst the rat was under isoflurane anesthesia. The PET data acquisition was conducted for 10 min, beginning 50 min after the ^{18}F-FDG injection. Using a lamp, the body temperature of the rats was maintained at between 36 and 37˚C during the scan. The images were reconstructed using a 3D maximum *a posteriori* (18 iterations with 16 subsets; β=0.2), without attenuation correction. The tracer uptake was expressed as the standardized uptake value (SUV).

Subsequent to PET scanning, plain or contrast-enhanced CT (CECT) was conducted with an X-ray source set at 90 kVp and 200 μA, using a small-animal CT system (R_mCT2; Rigaku, Tokyo, Japan). For CECT, the rats were intravenously injected with 10 ml Iopamiron 370 contrast medium (Bayer Yakuhin Ltd., Osaka, Japan) using an infusion pump (NE-1000; Neuroscience Inc., Tokyo, Japan) at the rate of 2 ml/min, whilst the rats were under isoflurane anesthesia. The CECT images were acquired 5 min subsequent to the injection. In order to reduce the motion artifacts caused by respiratory and peristaltic movement during the CT scan, a respiratory gating system was used whilst the rats under inhalable isoflurane anesthesia. The ^{18}F-FDG-PET scanning was conducted at two, three, four, five and eight weeks subsequent to administration of the Cre-expressing adenovirus or the empty vectors. In order to confirm the results of the PET analysis, the CECT scan was also conducted at five and eight weeks subsequent to the virus injection. For the quantitative analysis, the PET and CT data sets were imported and the fused images were then obtained using ASIPro VM software (CTI Concorde Microsystems, Knoxville, TN, USA). Laparotomy was performed six weeks subsequent to the injection in order to confirm the location and size of the pancreatic tumors, which were visible to the naked eye. The experimental rats were sacrificed eight weeks subsequent to the injection.

Histopathological examination. The rats in groups 1 and 2 survived until the end of the experimental period. The pancreatic tumors and the normal pancreatic lobes were removed from the abdomen of the rats, fixed with 10% buffered formalin and then processed for histopathological examination using hematoxylin and eosin stain (9). The pancreatic lesions were diagnosed histopathologically based upon previously described criteria (8,9).

Results

PET/CT findings and histopathological examination. The six rats were euthanized eight weeks subsequent to the injection of the Cre-expressing viral or empty vectors. All three Cre-expressing transgenic rats in group 1 (100%) developed orthotopic pancreatic tumors without distant metastasis. By contrast, no tumors were identified in the negative control rats of group 2. Upon macroscopic analysis, the tumors appeared nodular and solid in shape, and were ochre yellow in color. The

Table I. Mean SUV of the tumor and each organ in the experimental rats.

Rat	Tumor (SUV_{max})	GI tract (SUV_{max})	Liver	Kidney (cortex and medulla)
1	0.7-1.2 (1.4)	0.5-1.0 (3.2)	0.4-0.5	0.8-0.9
2	0.9-2.0 (3.0)	0.5-1.8 (2.7)	0.5-0.6	0.9-1.1
3	ND	0.6-1.4 (4.2)	0.6-0.7	0.9-1.1

The rats were inoculated with a Cre recombinase-expressing vector as described in the Materials and methods section. The values were calculated using the scanning data obtained at eight weeks post-inoculation. SUV_{max}, maximum standardized uptake value; GI, gastrointestinal; ND, Not detected.

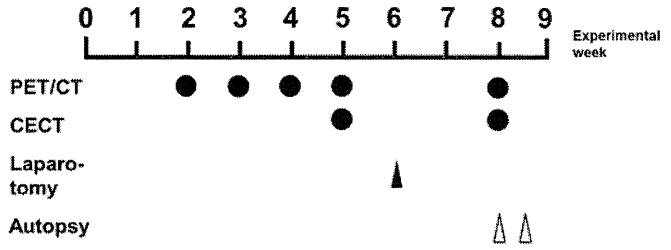

Figure 1. Experimental time course. Closed circle indicates the time of scanning. Closed triangle indicates the time of laparotomy. Open triangle indicates the time of autopsy. Laparotomy and autopsy were performed on the three rats from group 1 at eight weeks post-viral inoculation. Viral inoculation was performed at week zero. PET, positron emission tomography; CT, computed tomography; CECT, contrast-enhanced computed tomgraphy.

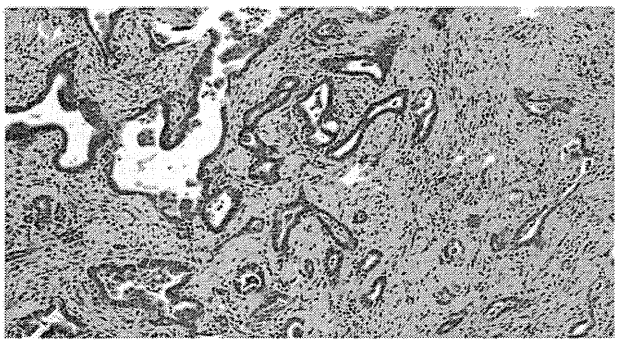

Figure 2. Representative microscopic image of a pancreatic ductal adenocarcinoma, revealing papillotubular growth of the tumor cells and abundant fibrous tissue proliferation (hematoxylin and eosin staining; magnification, x100).

PET/CT images obtained eight weeks subsequent to the viral injection revealed the majority of tumor tissues to be distinguishable from the adjacent organs, but the tissues were challenging to distinguish from the normal intestinal tissues, depending on the site of the tumor. The pancreatic tumors were of the ductal adenocarcinoma histological type. The coexistence of adenocarcinoma and PanIN lesions surrounded by fibrous tissue with inflammatory cell infiltration was also identified (Fig. 2).

[^{18}F-FDG-PET imaging prior to experimental week five. The representative maximal-intensity projection images from ^{18}F-FDG-PET are shown in Fig. 3. PET scanning was performed four times prior to the five experimental weeks. A marginal or very high uptake in the gastrointestinal tract and urinary bladder, which was considered to be physiological FDG uptake, was observed in all three Cre-expressing transgenic rats and three control rats. At five weeks post-treatment, the tumors were not clearly visualized by the indicated imaging system. Following the laparotomy at six weeks post-treatment, a few small nodules measuring between 1 and 2 mm in diameter, indicative of a carcinoma, were identified in the pancreas of all Cre-expressing transgenic rats. No metastases were identified in the rats of the negative control group.

Analysis of CECT, PET and PET/CT images at eight weeks post-treatment. Representative slices of the ^{18}F-FDG-PET/CT fusion images obtained from the Cre-expressing transgenic rats are shown in Figs. 4-6. The SUV_{max} and SUV_{mean} of the pancreatic tumors and each organ are shown in Table I. In rat 1 (body weight, 503 g), the CECT images revealed a heterogeneous lesion measuring 17 mm in the maximum sagittal diameter in the left side of the abdomen. In addition, the PET and PET/CT fusion images revealed moderately increased ^{18}F-FDG uptake in the lesion located in the left side of the abdomen, with a SUV_{max} of <1.5. Physiological FDG uptake was observed in the gastrointestinal tract, and the SUV_{max} of this organ site was 3.2, as shown in Table I. Autopsy revealed a large tumor in the splenic lobe, which was detected by CECT and PET/CT. However, multiple tumors that were present in the duodenal lobe of the pancreas were not revealed by CECT and PET/CT (Fig. 4). In rat 2 (body weight, 470 g), the CECT images revealed a heterogeneously-enhanced pancreatic tumor, measuring 20 mm in the maximum sagittal diameter, in the left side of the abdomen. PET/CT fusion images revealed moderate uptake of ^{18}F-FDG (SUV_{max}, 3.0) in the pancreatic tumor. In addition, physiological FDG uptake in the gastrointestinal tract (SUV_{max}, 2.7) was observed. During autopsy, a large tumor in the splenic lobe was identified by the imaging analysis. In addition, multiple tumors were identified in the duodenal lobe of the pancreas, but these tumors were not visualized on CECT and PET/CT (Fig. 5). In rat 3 (body weight, 564 g), the presence of a tumor was not observed on either CECT or PET scans (Fig. 6). Next, an incision was made in the abdomen of the rat, and a number of nodules, which were smaller in size than those observed in rats no. 1 and 2, were identified in the

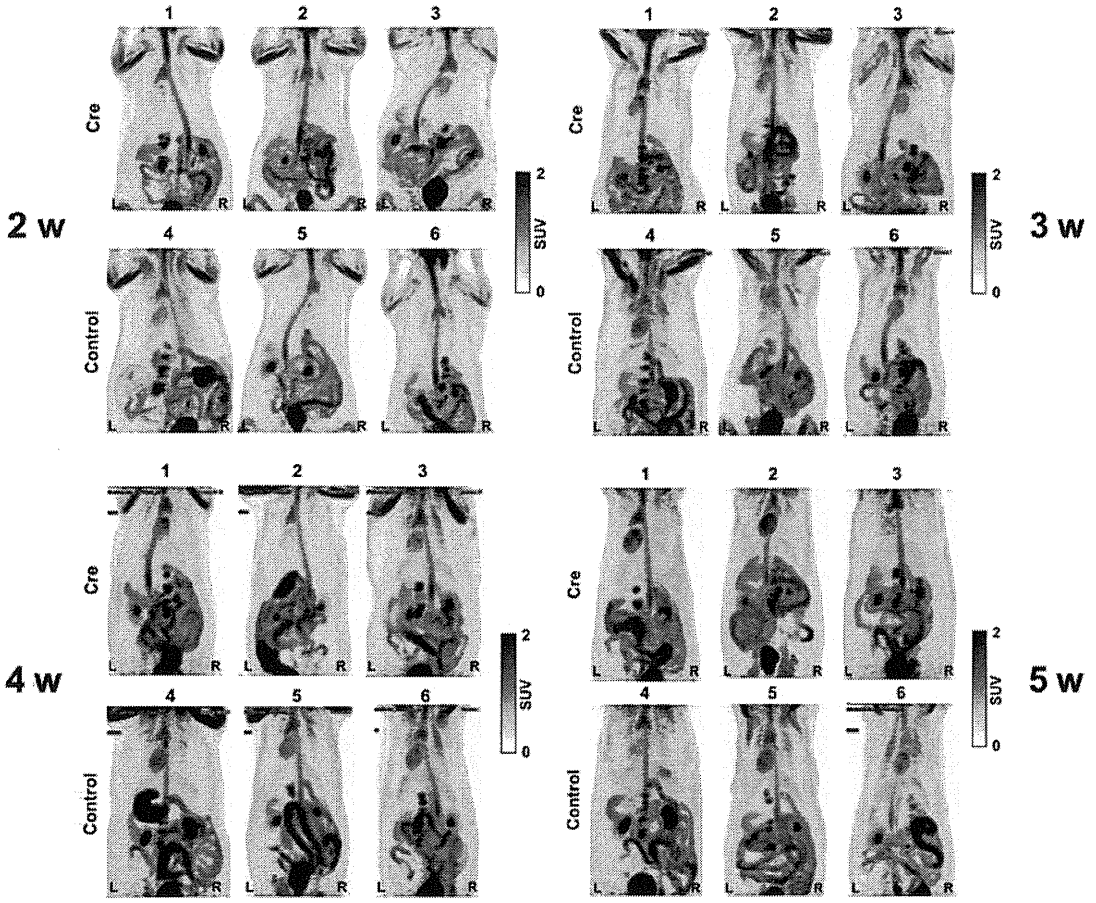

Figure 3. Representative positron emission tomography (PET) images of the transgenic rats at a maximum intensity projection. Images were obtained from Cre recombinase (Cre)-expressing transgenic rats (1-3) and control rats (4-6). Scanning was performed at two, three, four and five weeks post-viral inoculation. Subsequent to fasting, the rats were injected under isoflurane anesthesia with ~15 MBq ^{18}F-fluorodeoxyglucose (FDG) via the tail vein. PET data was acquired 50 min post-injection. Physiological FDG uptake was observed in the intestines, kidney and urinary bladder, but no tumor masses were identified in any of the images. L, left side; R, right side. SUV, standardized uptake value; w, weeks.

duodenal lobe of the pancreas. No tumor was identified in the splenic lobe of the pancreas. No macroscopic metastasis was identified in rats 1-3.

Discussion

A limited number of the documented studies that involve imaging analysis of pancreatic tumors in animal models used the FDG-PET/CT system (18,19). In the present study, a *KRAS*-mediated transgenic rat model was used to develop multiple pancreatic tumors that resembled the developmental and histological features of human PDAC within two weeks (8). In living rats at eight weeks post-treatment, the pancreatic tumors were clearly enhanced in the CECT images following the administration of a contrast media, and were distinguishable from the gastrointestinal tract. In the absence of imaging analysis, calipers are used to determine the location and size of a pancreatic tumor following a laparotomy or autopsy of an animal. Imaging analysis therefore allows each animal to be scanned sequentially in a sectional plane of interest, such as transverse, coronal or sagittal, and be monitored over time without the need to be sacrificed. In addition, PET/CT enables the accurate measurement of irregularly-shaped tumors in a pancreatic tumor model. According to the Three Rs principle (20), which aims to replace existing experimental methods with those that do not use animals, reduce the number of test animals used and refine methods in order to minimize the suffering of test animals, the PET/CT system reduces the number of animals required for experimental treatment and control groups. This indicates that imaging systems should be recommended for use in animal experiments. Recently, inoculation efficacy has been improved by clamping the common bile duct and increasing the amount of virus that is administered. Using this technique, studies may be able to control the size of the pancreatic tumor quantitatively within an appropriate time period, a factor that demonstrates the usefulness of this model.

With regard to studies that have used small animal models, Kitahashi *et al* (21) used micro-CT to detect chemically-induced pancreatic tumors of >4 mm in diameter in Syrian hamsters. Another study by Fendrich *et al* (18) detected precursor pancreatic adenocarcinoma lesions with an activity of 9.6±0.5 MBq in a five-month-old transgenic mouse model by FDG-PET/CT. Kayed *et al* (22) measured the anticancer effects of cyclopamine in a pancreatic carcinoma xenograft with an activity of 7.4 MBq model using ^{18}F-PET/CT. The study examined the size and SUV of each

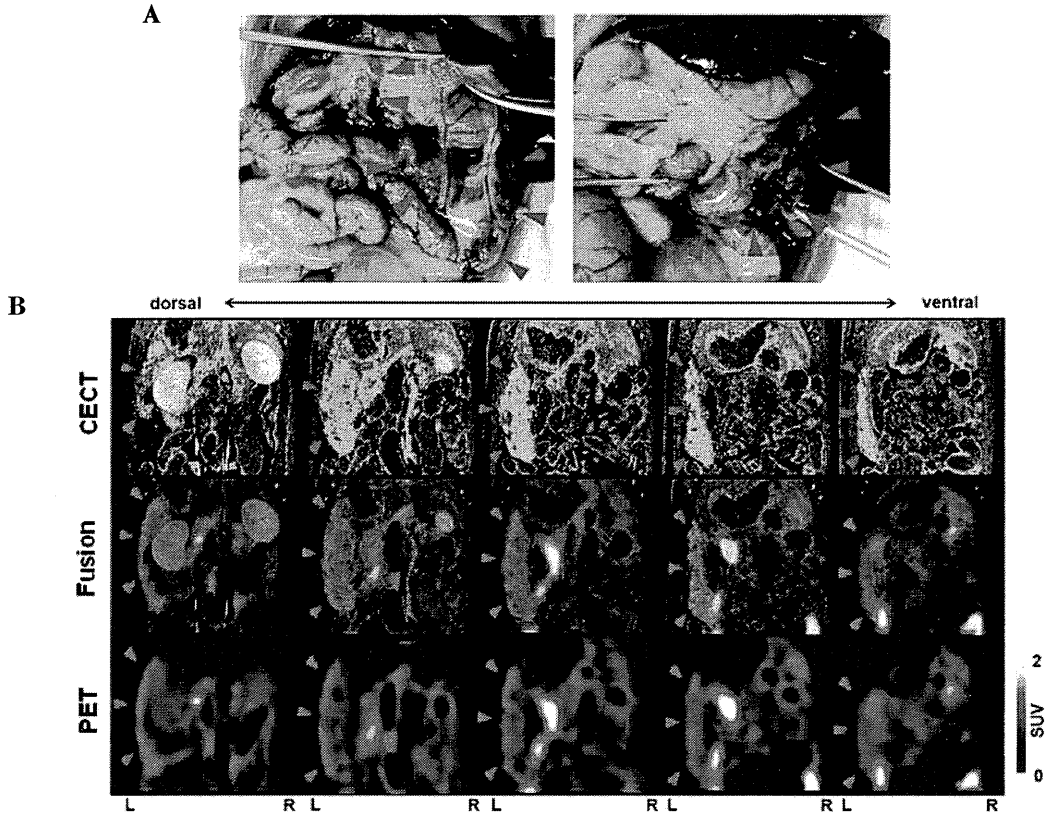

Figure 4. Autopsy view, positron emission tomography (PET)/contrast-enhanced CT (CECT) and PET/CECT fusion images of rat 1. (A) Tumors were observed in the duodenal lobe (left panel, red arrowheads) and the in splenic lobe (left and right panel, blue arrowheads) of the pancreas. (B) PET, CECT and PET/CECT fusion images revealed a large mass on the left side of the body (arrowheads). Physiological fluorodeoxyglucose uptake was also observed in the kidneys and intestines. L, left side; R, right side; SUV, standardized uptake value.

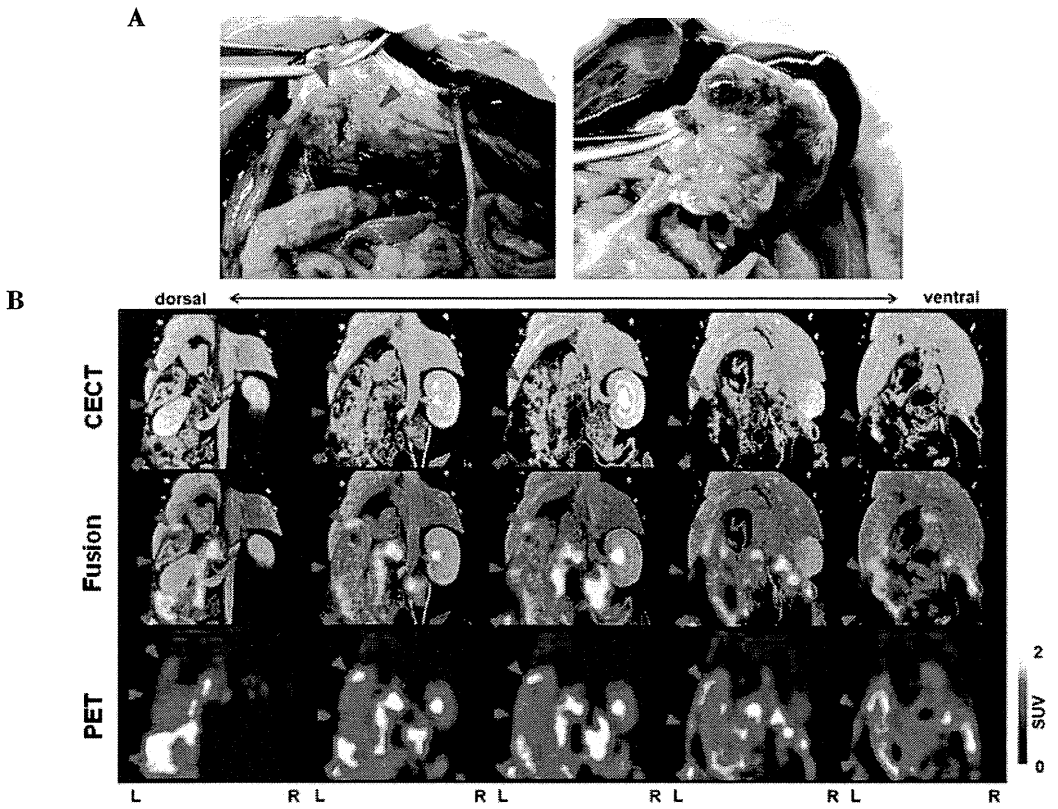

Figure 5. Autopsy view, positron emission tomography (PET), contrast-enhanced CT (CECT) and PET/CECT fusion images of rat 2. (A) Tumors were observed in the duodenal lobe (left and right panels, arrowheads) of the pancreas. The liver was intact. (B) PET, CECT and PET/CECT fusion images revealed multiple tumor masses in the left side of the body (arrowheads). L, left side; R, right side; SUV, standardized uptake value.

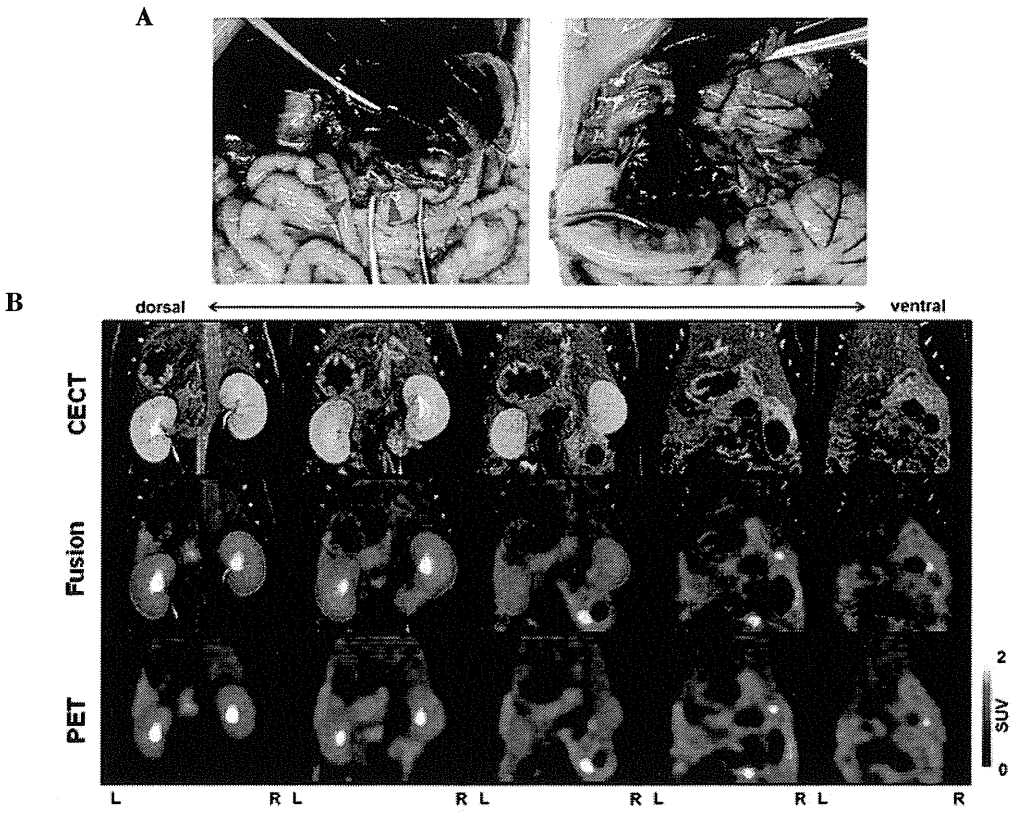

Figure 6. Autopsy view, positron emission tomgraphy (PET), contrast-enhanced CT (CECT) and PET/CECT fusion images of rat 3. (A) Tumors were observed in the duodenal lobe (left panel, arrowheads), but not in the splenic lobe of the pancreas. (B) No tumor-like lesions were revealed in the PET/CT and CECT images. SUV, standardized uptake value; R, right side; L, left side.

tumor that was grown in the hip region of nude mice during a seven-day treatment period. A technical limitation in baseline calibration occurred, but the system was believed to be suitable for practical use. The SUV and SUV_{max} parameters have been demonstrated in a previous study to be potential predictors of early recurrence following the curative resection of lung carcinomas (23).

It was hypothesized that the amount of FDG uptake into the pancreatic tumors would be higher compared with other abdominal organs. However, the results shown in Table I indicate that each value was not necessarily specific to the region of interest. This indicates a limitation in the use of this parameter for differential diagnoses that are based upon imaging techniques. To avoid bias during the measurement of the SUV, representative areas of tumor tissues that demonstrated moderate FDG uptake were selected. Therefore, the potential limitations of this methodology should be considered when calculating the SUV or SUV_{max}. This aspect warrants further investigation.

PET images did not identify tumor masses in any organ of the Cre-expressing rats until five weeks post-treatment (Fig. 3). When the laparotomy was performed six weeks subsequent to the viral inoculation, multiple tumors measuring <2 mm in diameter were identified in the pancreas of all three Cre-expressing transgenic rats. This indicated that the transgenic rats developed macroscopically visible tumors by six weeks post-treatment. At eight weeks post-treatment, the PET/CT images revealed pancreatic tumor masses in two of the three rats, which indicated a potential limitation in the detection of tumors prior to the eighth week by current imaging techniques. Pancreatic tumors were primarily identified in the splenic lobe of the pancreas by PET/CT. Tumors in the duodenal lobe, however, could not be detected by such imaging analyses, even if these tumors were confirmed by laparotomy. In addition, the presence of smaller tumors, and a specific anatomical location within the gastrointestinal tract, may affect the visibility of the tumor. In the PET and PET/CT fusion images, the pancreatic tumors were visible, but the physiological ^{18}F-FDG uptake in the intestine reduced the appearance of the lesions.

In conclusion, the present study demonstrated that pancreatic tumors can be detected in rats using imaging modalities eight weeks after viral inoculation. The FDG-PET/CT imaging system is a valuable approach for the evaluation of the carcinogenic process and potential treatment or prevention methods for pancreatic tumors in mammalian models. Therefore, it is proposed that this experimental system can also be applied to studies that examine cases of human PDAC.

Acknowledgements

The authors would like to thank Maki Okada for providing technical assistance with the CECT scanning, Hidekatsu Wakizaka for providing operational and quality control support for the PET system and Nobuyuki Miyahara for providing quality control support for the CT system.

References

1. Ferlay J, Shin HR, Bray F, Forman D, Mathers C and Parkin DM: Estimates of worldwide burden of cancer in: GLOBOCAN 2008. Int J Cancer 127: 2893-2917, 2010.
2. Matsuda A, Matsuda T, Shibata A, Katanoda K, Sobue T and Nishimoto H; Japan Cancer Surveillance Research Group: Cancer incidence and incidence rates in Japan in 2007: a study of 21 population-based cancer registries for the Monitoring of Cancer Incidence in Japan (MCIJ) project. Jpn J Clin Oncol 43: 328-336, 2013.
3. Bosetti C, Bertuccio P, Negri E, La Vecchia C, Zeegers MP and Boffetta P: Pancreatic cancer: overview of descriptive epidemiology. Mol Carcinog 51: 3-13, 2012.
4. Cubilla AL and Fitzgerald PJ: Cancer of the exocrine pancreas: the pathologic aspects. CA Cancer J Clin 35: 2-18, 1985.
5. Morohoshi T, Held G and Klöppel G: Exocrine pancreatic tumours and their histological classification. A study based on 167 autopsy and 97 surgical cases. Histopathology 7: 645-661, 1983.
6. Wolfgang CL, Herman JM, Laheru DA, *et al:* Recent progress in pancreatic cancer. CA Cancer J Clin 63: 318-348, 2013.
7. Siegel R, Naishadham D and Jemal A: Cancer statistics. CA Cancer J Clin 63: 11-30, 2013.
8. Fukamachi K, Tanaka H, Hagiwara Y, *et al:* An animal model of preclinical diagnosis of pancreatic ductal adenocarcinomas. Biochem Biophys Res Commun 390: 636-641, 2009.
9. Ueda S, Fukamachi K, Matsuoka Y, *et al:* Ductal origin of pancreatic adenocarcinomas induced by conditional activation of a human Ha-ras oncogene in rat pancreas. Carcinogenesis 27: 2497-2510, 2006.
10. Yabushita S, Fukamachi K, Tanaka H, *et al:* Metabolomic and transcriptomic profiling of human K-ras oncogene transgenic rats with pancreatic ductal adenocarcinomas. Carcinogenesis 34: 1251-1259, 2013.
11. Yabushita S, Fukamachi K, Kikuchi F, *et al:* Twenty-one proteins up-regulated in human H-ras oncogene transgenic rat pancreas cancers are up-regulated in human pancreas cancer. Pancreas 42: 1034-1039, 2013.
12. Yabushita S, Fukamachi K, Tanaka H, *et al:* Circulating microRNAs in serum of human K-ras oncogene transgenic rats with pancreatic ductal adenocarcinomas. Pancreas 41: 1013-1018, 2012.
13. Asagi A, Ohta K, Nasu J, *et al:* Utility of contrast-enhanced FDG-PET/CT in the clinical management of pancreatic cancer: impact on diagnosis, staging, evaluation of treatment response, and detection of recurrence. Pancreas 42: 11-19, 2013.
14. Tomimaru Y, Takeda Y, Tatsumi M, *et al:* Utility of 2-[18F] fluoro-2-deoxy-D-glucose positron emission tomography in differential diagnosis of benign and malignant intraductal papillary-mucinous neoplasm of the pancreas. Oncol Rep 24: 613-620, 2010.
15. Lan BY, Kwee SA and Wong LL: Positron emission tomography in hepatobiliary and pancreatic malignancies: a review. Am J Surg 204: 232-241, 2012.
16. Studwell AJ and Kotton DN: A shift from cell cultures to creatures: in vivo imaging of small animals in experimental regenerative medicine. Mol Ther 19: 1933-1941, 2011.
17. Kanegae Y, Lee G, Sato Y, *et al:* Efficient gene activation in mammalian cells by using recombinant adenovirus expressing site-specific Cre recombinase. Nucleic Acids Res 23: 3816-3821, 1995.
18. Fendrich V, Schneider R, Maitra A, Jacobsen ID, Opfermann T and Bartsch DK: Detection of precursor lesions of pancreatic adenocarcinoma in PET-CT in a genetically engineered mouse model of pancreatic cancer. Neoplasia 13: 180-186, 2011.
19. van Kouwen MC, Laverman P, van Krieken JH, Oyen WJ, Jansen JB and Drenth JP: FDG-PET in the detection of early pancreatic cancer in a BOP hamster model. Nucl Med Biol 32: 445-450, 2005.
20. Russell WMS and Burch RL (eds): The Principles of Humane Experimental Technique. 2nd edition. Methuen & Co, London, 1992.
21. Kitahashi T, Mutoh M, Tsurusaki M, *et al:* Imaging study of pancreatic ductal adenocarcinomas in Syrian hamsters using X-ray micro-computed tomography (CT). Cancer Sci 101: 1761-1766, 2010.
22. Kayed H, Meyer P, He Y, *et al:* Evaluation of the metabolic response to cyclopamine therapy in pancreatic cancer xenografts using a clinical PET-CT system. Transl Oncol 5: 335-343, 2012.
23. Sakai T, Tsushima T, Kimura D, Hatanaka R, Yamada Y and Fukuda I: A clinical study of the prognostic factors for postoperative early recurrence in patients who underwent complete resection for pulmonary adenocarcinoma. Ann Thorac Cardiovasc Surg 17: 539-543, 2011.

Multiwalled carbon nanotubes intratracheally instilled into the rat lung induce pleural malignant mesothelioma and lung tumors

Journal:	*Cancer Science*
Manuscript ID	CAS-OA-0169-2016.R1
Manuscript Type:	Original Article
Date Submitted by the Author:	17-Apr-2016
Complete List of Authors:	Suzui, Masumi; Nagoya City University Graduate School of Medical Sciences, Molecular Toxicology Futakuchi, Mitsuru; Nagoya City University Graduate School of Medical Sciences, Molecular Toxicology Fukamachi, Katsumi; Nagoya City University Graduate School of Medical Sciences, Molecular Toxicology Numano, Takamasa; Nagoya City University Graduate School of Medical Sciences, Molecular Toxicology Abdelgied, Mohamed; Nagoya City University, Nanotoxicology Project; Nagoya City University Graduate School of Medical Sciences, Experimental Pathology and Tumor Biology; Beni Suef University, Forensic Medicine and Toxicology, Faculty of Veterinary Medicine Takahashi, Satoru; Nagoya City University Graduate School of Medical Sciences, Experimental Pathology and Tumor Biology Ohnishi, Makoto; Japan Industrial Safety and Health Association Japan Bioassay Research Center Omori, Toyonori; National Center for Child Health and Development Tsuruoka, Shuji; Shinshu University, Institute of Carbon Science & Technology Hirose, Akihiko; National Institute of Health Sciences, Risk Assessment, Biological Safety Research Center Kanno, Jun; National Institute of Health Sciences, Division of Cellular and Molecular Toxicology Sakamoto, Yoshimitsu; Tokyo Metropolitan Institute of Public Health, Environmental and Toxicology Alexander, David; Nagoya City University, Nanotoxicology Project Alexander, William; Nagoya City University, Nanotoxicology Project Xu, Jiegou; Anhui Medical University College of Basic Medical Sciences, Department of Immunology; Nagoya City University, Nanotoxicology Project Tsuda, Hiroyuki; Nagoya City University, Nanotoxicology Project
Keyword:	
Optional Keywords: please type five keywords that are identical to those described in	Multiwalled carbon nanotubes, intratracheal instillation, malignant mesothelioma, lung tumors, rat

the manuscript:	

Multiwalled carbon nanotubes intratracheally instilled into the rat lung induce development of pleural malignant mesothelioma and lung tumors

Masumi Suzui[1], Mitsuru Futakuchi[1], Katsumi Fukamachi[1], Takamasa Numano[1], Mohamed Abd Elgied [2,3,4], Satoru Takahashi[3], Makoto Ohnishi[5], Toyonori Omori[6], Shuji Tsuruoka[7], Akihiko Hirose[8], Jun Kanno[9], Yoshimitsu Sakamoto[10], David B. Alexander[2], William T. Alexander[2], Xu Jiegou[2,11]*, and Hiroyuki Tsuda[2]*

[1] Masumi Suzui
Nagoya City University Graduate School of Medical Sciences,
Department of Molecular Toxicology,
1 Kawasumi, Mizuho-cho, Mizuho-ku,
Nagoya 467-8601, Japan
suzui@med.nagoya-cu.ac.jp

[1] Mitsuru Futakuchi
Nagoya City University Graduate School of Medical Sciences,
Department of Molecular Toxicology,
1 Kawasumi, Mizuho-cho, Mizuho-ku,
Nagoya 467-8601, Japan
futakuch@med.nagoya-cu.ac.jp

[1] Katsumi Fukamachi
Nagoya City University Graduate School of Medical Sciences,
Department of Molecular Toxicology,
1 Kawasumi, Mizuho-cho, Mizuho-ku,
Nagoya 467-8601, Japan
kfukamac@med.nagoya-cu.ac.jp

[1] Takamasa Numano
Nagoya City University Graduate School of Medical Sciences,
Department of Molecular Toxicology,
1 Kawasumi, Mizuho-cho, Mizuho-ku,
Nagoya 467-8601, Japan
Numano@dims.co.jp

[2] Mohamed Abd Elgied
Nagoya City University,
Nanotoxicology Project
3-1 Tanabe-Dohri, Mizuho-ku,
Nagoya 466-8603, Japan
c151902@ed.nagoya-cu.ac.jp

[3] Mohamed Abd Elgied
Nagoya City University Graduate School of Medical Sciences,
Department of Experimental Pathology and Tumor Biology,
1 Kawasumi, Mizuho-cho, Mizuho-ku,
Nagoya 467-8601, Japan
c151902@ed.nagoya-cu.ac.jp

[4] Mohamed Abd Elgied
Beni-Suef University
Forensic Medicine and Toxicology,
Faculty of Veterinary Medicine,
Beni-Suef 62511
Egypt
m.abdelgaid@vet.bsu.edu.eg>

[3] Satoru Takahashi
Nagoya City University Graduate School of Medical Sciences,
Department of Experimental Pathology and Tumor Biology,
1 Kawasumi, Mizuho-cho, Mizuho-ku,
Nagoya 467-8601, Japan
sattak@med.nagoya-cu.ac.jp

[5] Makoto Ohnishi
Japan Industrial Safety and Health Association,
Japan Bioassay Research Center,
2445 Hirasawa, Hadano,
Kanagawa 257-0015, Japan
m-onishi@jisha.or.jp